Journal of Medicinal Chemistry

ARTICLE

pubs.acs.org/jmc

Binding of α,α-Disubstituted Amino Acids to Arginase Suggests New Avenues for Inhibitor Design†

Monica Ilies,[‡] Luigi Di Costanzo,[§] Daniel P. Dowling,[∥] Katherine J. Thorn,[⊥] and David W. Christianson*[,#]

[‡]Department of Chemistry, Drexel University, Philadelphia, Pennsylvania 19104-2875, United States

[§]RCSB Protein Data Bank, Department of Chemistry and Chemical Biology, Rutgers The State University of New Jersey, Piscataway, New Jersey 08854-8087, United States

[∥]Department of Chemistry, Massachusetts Institute of Technology, Cambridge, Massachusetts 02139-4307, United States

[⊥]The Episcopal Academy, Newtown Square, Pennsylvania 19073, United States

[#]Roy and Diana Vagelos Laboratories, Department of Chemistry, University of Pennsylvania, Philadelphia, Pennsylvania 19104-6323 United States

ABSTRACT: Arginase is a binuclear manganese metalloenzyme that hydrolyzes L-arginine to form L-ornithine and urea, and aberrant arginase activity is implicated in various diseases such as erectile dysfunction, asthma, atherosclerosis, and cerebral malaria. Accordingly, arginase inhibitors may be therapeutically useful. Continuing our efforts to expand the chemical space of arginase inhibitor design and inspired by the binding of 2-(difluoromethyl)-L-ornithine to human arginase I, we now report the first study of the binding of α,α-disubstituted amino acids to arginase. Specifically, we report the design, synthesis, and assay of racemic 2-amino-6-borono-2-methylhexanoic acid and racemic 2-amino-6-borono-2-(difluoromethyl)hexanoic acid. X-ray crystal structures of human arginase I and *Plasmodium falciparum* arginase complexed with these inhibitors reveal the exclusive binding of the L-stereoisomer; the additional α-substituent of each inhibitor is readily accommodated and makes new intermolecular interactions in the outer active site of each enzyme. Therefore, this work highlights a new region of the protein surface that can be targeted for additional affinity interactions, as well as the first comparative structural insights on inhibitor discrimination between a human and a parasitic arginase.

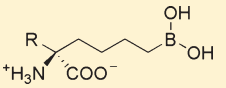

INTRODUCTION

Arginase is a ubiquitous manganese metalloenzyme that catalyzes the hydrolysis of L-arginine to form L-ornithine and urea. In mammals, two isozymes have been identified with distinct tissue distributions and subcellular localizations.[1−5] Arginase I is a cytosolic enzyme found predominantly in the liver, and arginase II is a mitochondrial enzyme found at highest concentrations in the kidney.[6−9] However, both isozymes are constitutively expressed or induced in other tissues to regulate cationic amino acid homeostasis in three critical metabolic pathways: (1) the regulation of L-arginine levels for nitric oxide (NO) biosynthesis;[10−15] (2) the regulation of L-ornithine levels for L-proline biosynthesis to promote collagen production;[16,17] (3) the regulation of L-ornithine levels for polyamine biosynthesis to facilitate cellular proliferation.[2,18−20]

Significantly, expression of arginase I and/or arginase II is up-regulated in certain diseased tissues and cell types. For example, given that arginase competes with NO synthase for their common substrate L-arginine, aberrant arginase II activity in the penile corpus cavernosum of the diabetic male attenuates NO biosynthesis and therefore compromises the NO-dependent relaxation of cavernosal smooth muscle required for penile erection.[21] Moreover, arginase I levels in the corpus cavernosum increase with age and similarly compromise penile erection.[22] Thus, erectile dysfunction can result from the up-regulation of either arginase I or arginase II in different etiologies of the same disease. In another example, arginase I is up-regulated in the asthmatic lung by Th2 cytokines such as interleukin-13,[23−27] and arginase I and arginase II single-nucleotide polymorphisms are identified in atopic asthma.[28,29] Arginase activity contributes to asthma pathology through three metabolic functions:[30−32] (1) arginase compromises NO-dependent relaxation of airway smooth muscle, leading to bronchoconstriction; (2) arginase enhances L-proline and collagen biosynthesis, leading to the accumulation of fibrotic tissue in the chronic asthmatic airway; (3) arginase enhances polyamine biosynthesis, which stimulates cellular proliferation and hyperplasia, e.g., of airway smooth muscle cells, in the asthmatic airway. These disease manifestations can be blocked by the use of arginase inhibitors in ex vivo and in vivo experiments.[15,21,22,33−35] Thus, the arginase isozymes are increasingly considered as vital pharmaceutical targets for the treatment of erectile dysfunction, asthma, and cardiovascular diseases linked to aberrant arginase activity, such as atherosclerosis.[36]

The first high-affinity inhibitor of arginase to be reported was the boronic acid analogue of L-arginine, 2-(*S*)-amino-6-borono-hexanoic acid (ABH, Figure 1),[37] which binds to human arginase I (HAI) with K_d = 5 nM and human arginase II with K_i = 8.5 nM.[38,39] ABH is also the most potent inhibitor known for *Plasmodium falciparum* arginase (PFA), to which it binds more weakly with K_d = 11 μM.[40] The X-ray crystal structures of HAI and rat arginase I complexed with ABH,[15,38] as well as the

Received: April 13, 2011
Published: July 05, 2011

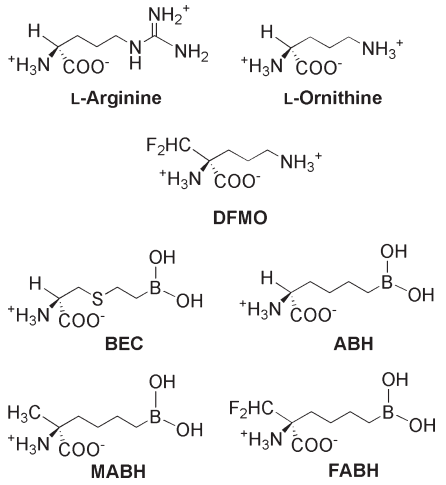

Figure 1. The amino acid substrate and product of the reaction catalyzed by arginase, L-arginine and L-ornithine respectively, are compared with DFMO and the boronic acid inhibitors BEC, ABH, MABH, and FABH.

structure of the PFA−ABH complex,[40] reveal that the boronic acid side chain undergoes nucleophilic attack by the metal-bridging hydroxide ion observed in the unliganded enzyme[41,42] to yield a tetrahedral boronate anion that mimics the tetrahedral intermediate and its flanking transition states in catalysis. The binding of the ABH analogue *S*-(2-boronoethyl)-L-cysteine (BEC, Figure 1) to HAI and human arginase II occurs through an identical mechanism.[33,38]

Structural comparisons of arginase−ABH and −BEC complexes reveal a conserved hydrogen bond network responsible for the molecular recognition of the inhibitor α-amino and α-carboxylate groups; these interactions contribute significantly to enzyme−inhibitor affinity, as demonstrated in recent mutagenesis studies with rat arginase I.[43] Given that ABH analogues in which the side chain is modified exhibit radically diminished affinity,[37,44,45] there is only one remaining possibility for the derivatization of the ABH scaffold to yield new inhibitors: the amino acid Cα-H atom, which in the enzyme−inhibitor complex is solvent exposed and oriented toward a region of the protein surface that is currently "uncharted" with regard to inhibitor binding. The design and synthesis of α,α-disubstituted amino acids based on the high-affinity ABH scaffold (Figure 1) may thus enable the generation and development of a new class of arginase inhibitors to expedite the search for new arginase-directed therapies. Notably, such therapies may target indications beyond those outlined above. For instance, the inhibition of PFA has been recently proposed as a potential adjuvant therapy for accelerating the recovery of malaria patients.[40,46]

We now report the first study of the binding of α,α-disubstituted amino acids to arginase. We demonstrate initial proof-of-principle with the X-ray crystal structures of HAI complexed with 2-(difluoromethyl)-L-ornithine (DFMO) and L-ornithine to show that an additional α-substituent does not perturb the intermolecular interactions of the amino acid product of the arginase reaction. We then describe the design, synthesis, and assay of two new α,α-disubstituted derivatives of ABH: 2-amino-6-borono-2-methylhexanoic acid (MABH) and 2-amino-6-borono-2-(difluoromethyl)hexanoic acid (FABH) (Figure 1). X-ray crystal structures of their complexes with HAI and PFA, together with in vitro evaluations of inhibitory potency, illuminate new avenues toward the development of α,α-disubstituted amino acids as arginase inhibitors.

RESULTS

HAI−DFMO Complex. While DFMO is reported[47] to be a weak inhibitor of arginase activity in human colon carcinoma cells with K_i = 3.9 mM, and while racemic DFMO was used in crystal soaking experiments with HAI, the omit map in Figure 2a clearly shows that the L-stereoisomer of DFMO is bound exclusively with full occupancy. This reflects the stereoselectivity of the HAI active site for the binding of L-amino acids; e.g., L-arginine is a substrate for arginase, whereas D-arginine is not.[48] Inhibitor binding does not cause any significant conformational changes in the active site or elsewhere in the protein structure, and the rms deviation is 0.26 Å for 314 Cα atoms in comparison with the unliganded enzyme. As for DFMO, the catalytic product L-ornithine binds in the HAI active site without causing any significant conformational changes. The rms deviation is 0.22 Å for 314 Cα atoms in comparison with the unliganded enzyme. An omit map showing the binding of L-ornithine is found in Figure 2b. Comparison of the two complexes reveals a generally similar binding mode for DFMO and L-ornithine (Figure 2c). Direct and water-mediated hydrogen bonds with the α-amino and α-carboxylate groups are identical in each complex. These interactions are crucial affinity determinants,[43] and α,α-disubstitution clearly does not perturb them.

Chemistry. Since the active site of HAI readily accommodated the additional α-substituent of DFMO without perturbing the binding interactions or conformation observed for L-ornithine, we synthesized the corresponding α,α-disubstituted derivatives of the archetype HAI inhibitor, ABH (MABH and FABH; see Figure 1). As shown in Scheme 1, the key intermediate in the syntheses of MABH and FABH was ethyl 2-*N*-(diphenylmethyleneamino)hex-5-enoate (**2**). While this compound was previously reported,[49] we developed an alternative synthetic pathway with a comparable overall yield. We synthesized **2** from the commercially available *N*-(diphenylmethylene)glycine ethyl ester (**1**), using the classic mild deprotonation with potassium *tert*-butoxide (^{t}BuOK),[50,51] followed by alkylation with 4-bromo-1-butene. The use of benzophenone imines of glycine alkyl esters as precursors of α-amino acids is a well-known[52] synthetic strategy to ensure selective monoalkylation of the amino acid Cα atom. We employed the same mild base (^{t}BuOK) to further deprotonate the Cα in the resulting derivative **2**. Subsequent one-pot reaction with methyl iodide and chlorodifluoromethane[53] respectively yielded the corresponding methyl (**3**) and difluoromethyl (**4**) derivatives in good yields as new compounds (Scheme 1). Hydroboration with pinacolborane catalyzed by complexes of cyclooctadiene iridium chloride dimer, $[Ir(cod)Cl]_2$, with 1,1-bis(diphenylphosphino)-methane (dppm)[54] introduced the synthetic equivalent of the boronic synthon in the terminal olefins **3** and **4**, correspondingly generating the intermediates **5** and **6**. Complete deprotection of derivatives **5** and **6** with 6 N HCl in tetrahydrofuran (THF) led to the targeted compounds MABH (**7**) and FABH (**8**), respectively.

Binding Affinities of MABH and FABH. Dissociation constants for the *S*-isomer of ABH and racemic MABH and FABH against HAI determined by surface plasmon resonance (Figure 3) and inhibition constants against PFA determined by kinetic assay are recorded in Table 1. Curiously, both α,α-disubstituted derivatives of ABH exhibit weaker affinity compared with ABH. For HAI, MABH and FABH bind 49-fold and 1889-fold less

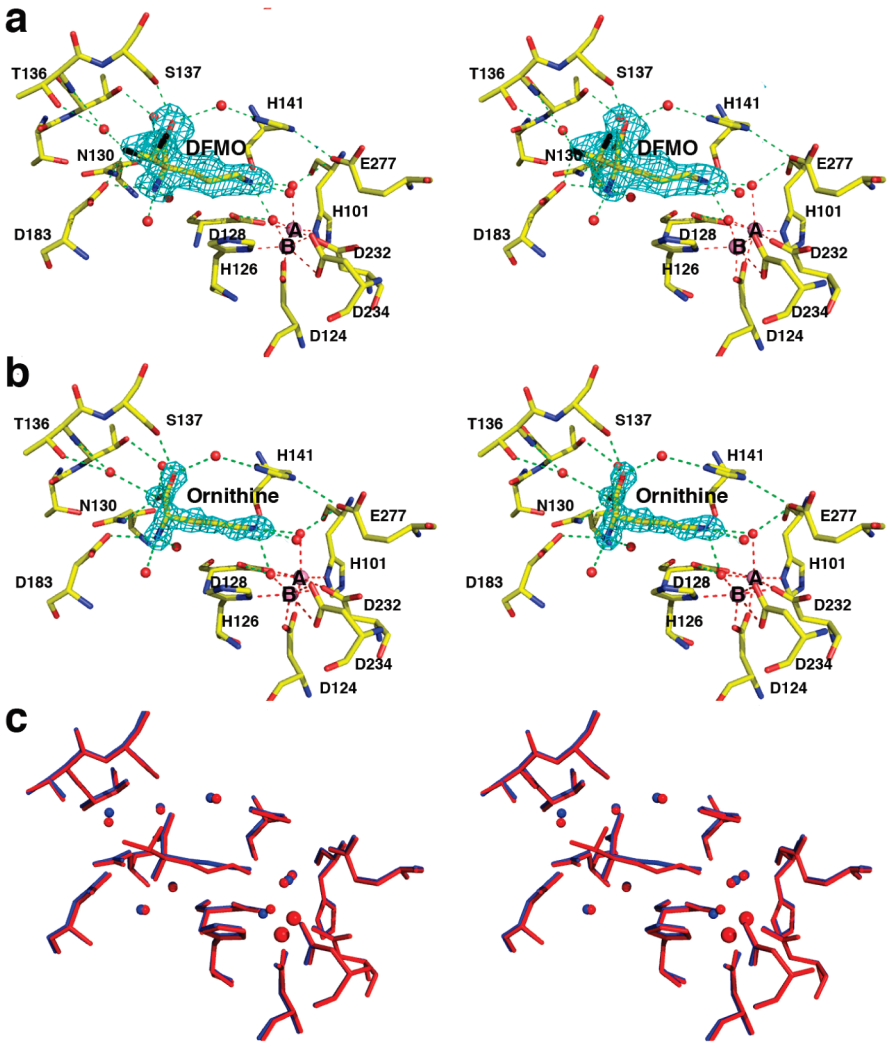

Figure 2. (a) Simulated annealing omit electron density map of the HAI—DFMO complex (cyan, contoured at 3.0σ), in which DFMO was omitted from the structure factor calculation. Atoms are color-coded as follows: C = yellow, O = red, N = blue, F = black; Mn^{2+} ions and water molecules are purple and red spheres, respectively. Metal coordination and hydrogen bond interactions are indicated by red and green dashed lines, respectively. (b) Simulated annealing omit electron density map of the HAI—L-ornithine complex (cyan, contoured at 3.3σ). Atoms are color-coded as in (a). (c) Superposition of the HAI—DFMO complex (red) and the HAI—L-ornithine complex (blue).

tightly, respectively; for PFA, MABH and FABH exhibit inhibitory potencies based on K_i that are 26-fold and 200-fold weaker than that observed for ABH. The structural basis for affinity loss is not immediately evident for the binding of α,α-disubstituted amino acids to HAI based on crystal structures of enzyme—inhibitor complexes; however, that only the L-stereoisomer of each inhibitor binds indicates that the affinity losses are only one-half those measured for the racemic mixture (vide infra). Even so, it is quite possible that affinity can be recaptured and enhanced with longer α-substituents capable of making favorable interactions in the active site. In contrast with HAI—inhibitor complexes, crystal structures of PFA—inhibitor complexes reveal intersubunit interactions with the α-substituents of MABH and FABH.

Crystal Structures of HAI—MABH and HAI—FABH Complexes. The 1.60 Å resolution crystal structure of the HAI—MABH complex reveals that inhibitor binding does not cause any significant conformational changes in the active site or elsewhere in the protein structure. The rms deviation is 0.24 Å for 313 Cα atoms in comparison with the HAI—ABH complex. The electron density of MABH is well-defined and clearly indicates that the L-stereoisomer of racemic MABH used in cocrystallization experiments is exclusively selected for binding in the HAI active site (Figure 4a). Superposition with the 1.29 Å resolution crystal structure of human arginase I—ABH complex shows excellent overlap (Figure 4c), and enzyme—inhibitor hydrogen bonds are identical in both complexes.

The 1.7 Å resolution electron density map of the HAI—FABH complex similarly reveals the exclusive binding of the L-stereoisomer of racemic FABH used in cocrystallization experiments (Figure 4b). Inhibitor binding does not cause any significant overall conformational changes in the HAI structure, and the rms deviation for 313 Cα atoms is 0.29 Å when compared with the structure of the HAI—ABH complex. However, each fluorine atom of the α-difluoromethyl group accepts hydrogen bonds from solvent molecules, which in turn donate hydrogen bonds to D183; additionally, it appears that T136 undergoes a 128° conformational change about side chain torsion angle χ_1 to accommodate the binding of one of these solvent molecules

dx.doi.org/10.1021/jm200443b |J. Med. Chem. 2011, 54, 5432–5443

Scheme 1. Synthesis of 2-Amino-6-borono-2-methylhexanoic Acid (MABH) and 2-Amino-6-borono-2-difluoromethylhexanoic Acid (FABH)

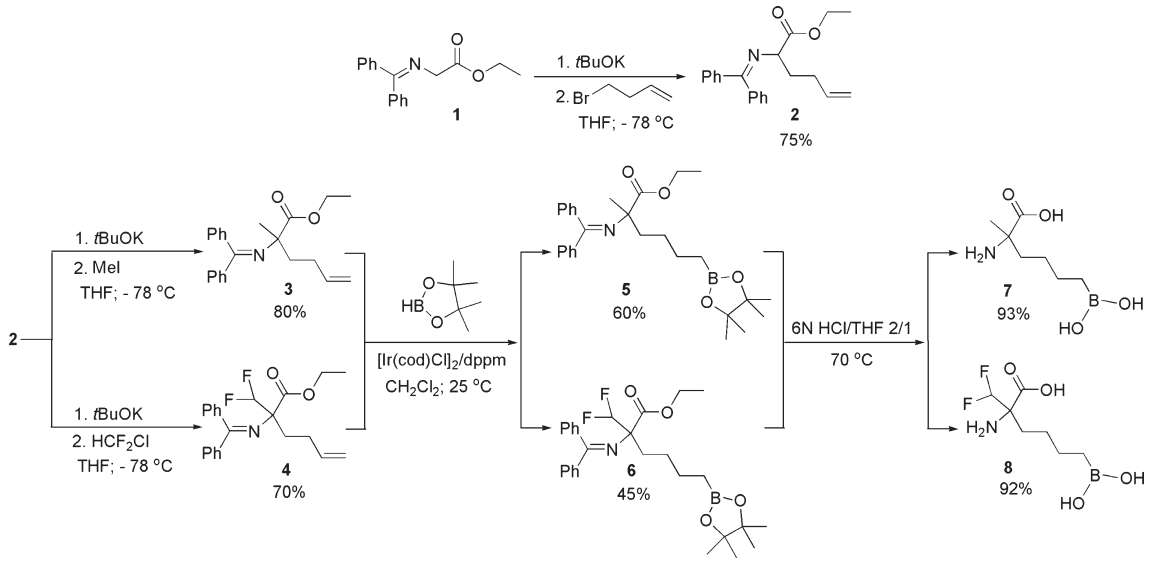

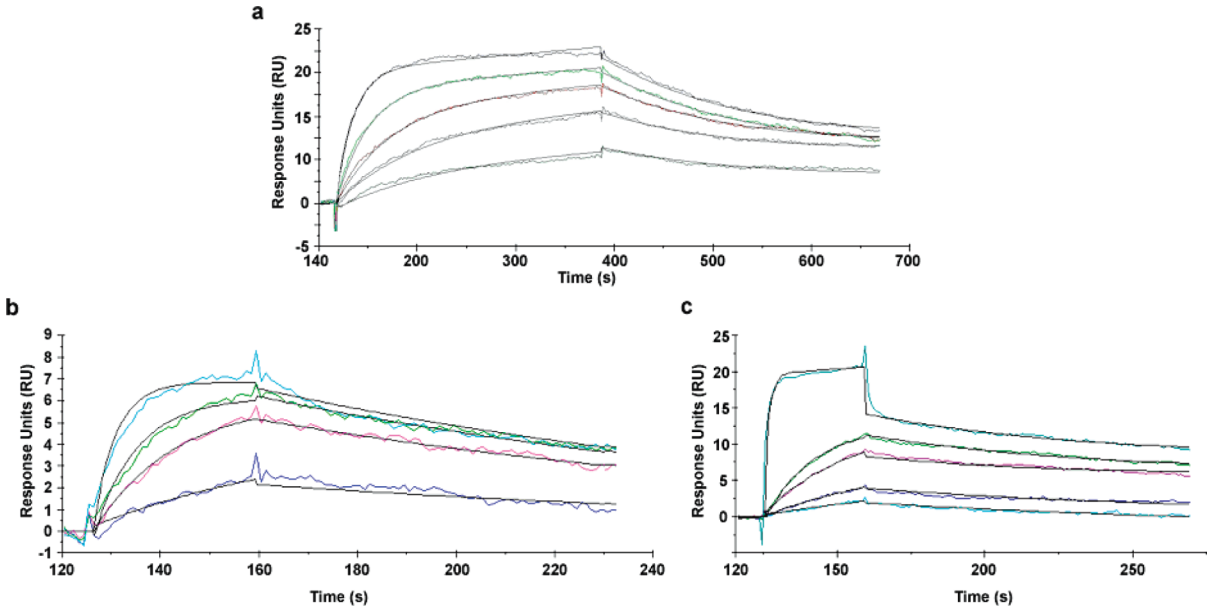

Figure 3. Surface plasmon resonance sensorgrams for HAI showing the binding of (a) ABH, $K_d = 18 \pm 1$ nM, (b) MABH, $K_d = 0.88 \pm 0.02$ μM, and (c) FABH, $K_d = 34 \pm 2$ μM.

(Figure 4c). Enzyme−inhibitor hydrogen bond interactions are otherwise identical to those observed in the HAI−ABH and HAI−MABH complexes.

Crystal Structures of PFA−MABH and PFA−FABH Complexes. The 1.9 Å resolution crystal structure of the PFA−MABH complex and the 2.0 Å resolution crystal structure of the PFA−FABH complex (Figure 5) each reveal the exclusive binding of the L-stereoisomer from the racemic inhibitor mixtures used in cocrystallization experiments. Surprisingly, however, each inhibitor binds to PFA with an intact boronic acid side chain; i.e., neither inhibitor binds in the tetrahedral boronate anion form as observed in the PFA−ABH complex[40] or in the HAI−MABH or HAI−FABH complex (Figure 4). Attempted refinement with the tetrahedral boronic acid form of each inhibitor resulted in negative electron density peaks on both the boron atom and the adjacent carbon atom. Such spurious peaks are not observed when each inhibitor is refined with an intact boronic acid moiety. Clear electron density for each inhibitor shows that a planar boronic acid moiety binds to preclude the binding of the metal-bridging solvent molecule typically observed in unliganded arginase structures.[41,42] Electron density for a water molecule coordinated to Mn_A^{2+} is ~2 Å from the boron atom of MABH and FABH (e.g., see Figure 5b). Thus, MABH and FABH do not bind as transition state analogues. Moreover, neither inhibitor

dx.doi.org/10.1021/jm200443b | J. Med. Chem. 2011, 54, 5432–5443

binds as a true substrate analogue, since the trigonal planar boronic acid moiety of each inhibitor adopts a binding conformation with a $C\delta-C\varepsilon-B\zeta-O\eta_1$ dihedral angle of ~90°, which is very different from the corresponding $C\delta-N\varepsilon-C\zeta-N\eta_1$ dihedral angle of 180° required by the planar guanidinium moiety of L-arginine. This structural aberration may contribute to the weaker affinity of MABH and FABH compared to ABH.

Inhibitor binding to PFA generally does not cause any significant conformational changes in the protein structure. However, active site solvent structure is slightly different in that the binding of α,α-disubstituted amino acids displaces a water molecule that is observed in the PFA—ABH complex (Figure 5d). In comparison with the PFA—ABH complex, the rms deviations are 0.10 Å for 308 Cα atoms and 0.12 Å for 308 Cα atoms for the PFA—MABH and PFA—FABH complexes, respectively. However, some local structural changes accommodate the binding of α,α-disubstituted amino acids. In particular, an alternative conformation with 50% occupancy is observed for D272 in the PFA—MABH complex; this residue hydrogen bonds with H381 in the PFA—ABH complex. The α-methyl group of MABH is 3.0 Å from the Nε2 atom of H381, and H381 rotates ~5° about side chain torsion angle χ_1, so this van der Waals contact may destabilize the H381—D272 interaction. Higher thermal *B* factors are observed for this portion of the inhibitor and the side chain of H381, suggesting that there is some residual disorder in this region of the enzyme—inhibitor complex.

Inhibitor binding conformations are very similar in PFA complexes with MABH and FABH (Figure 5d). Interestingly, the α-difluoromethyl group of FABH does not trigger the conformational change of D272 as observed in the PFA—MABH complex. H381 undergoes a slightly greater conformational change (~12°) than that observed in the PFA—MABH complex, perhaps due to a hydrogen bond interaction with one of the fluorine atoms of FABH (F···N separation of 2.6 Å). However, as observed in the PFA—MABH complex, higher thermal *B* factors characterize this portion of the inhibitor and the side chain of H381, suggestive of some residual disorder in this region of the enzyme—inhibitor complex. Such residual disorder may compromise enzyme—inhibitor affinity.

Table 1. α,α-Disubstituted Amino Acids Synthesized as Inhibitors of Human Arginase I (HAI) and *Plasmodium falciparum* Arginase (PFA)

inhibitor	HAI, K_d (μM)[a]	PFA, K_i (μM)[b]
ABH (*S*-isomer)	0.018 ± 0.001	10 ± 1[c]
MABH (racemic)[d]	0.88 ± 0.02	260 ± 20
FABH (racemic)[d]	34 ± 2	2000 ± 200

[a] Surface plasmon resonance. Errors are standard deviations of experiments run in triplicate. [b] Kinetic colorimetric assay. Errors are standard deviations of experiments run in triplicate. [c] From ref 40. [d] Since only the L-stereoisomer is observed to bind in each crystal structure, the actual K_d or K_i for the inhibitory stereoisomer is likely to be one-half that measured for the racemic mixture.

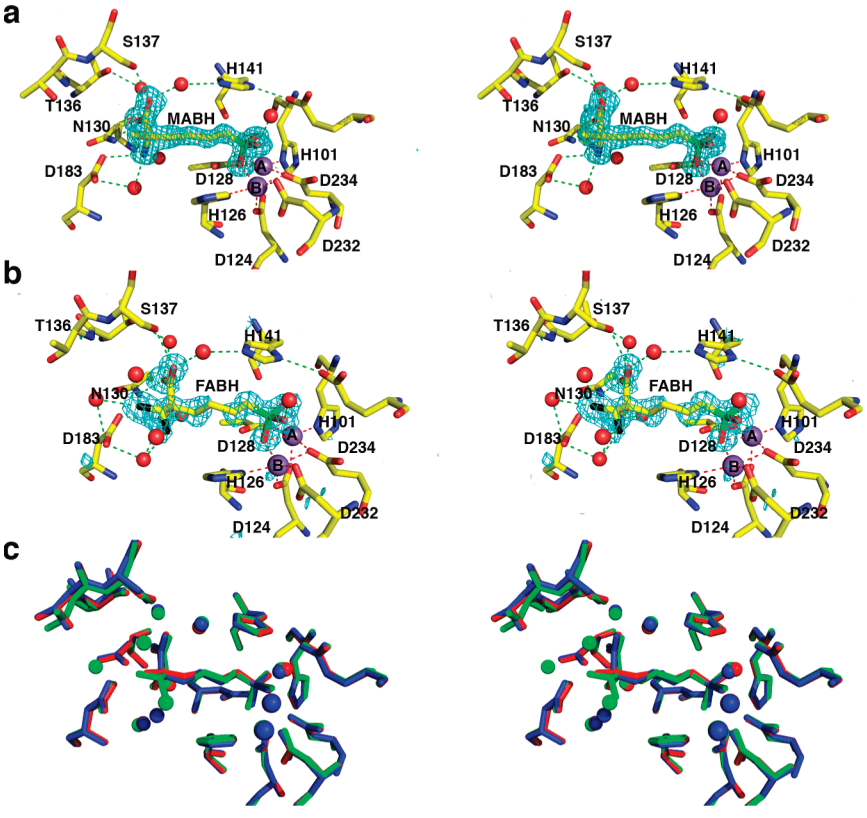

Figure 4. (a) Simulated annealing omit electron density map of the HAI—MABH complex (cyan, contoured at 3.8σ), in which MABH was omitted from the structure factor calculation. Atoms are color-coded as follows: C = yellow, O = red, N = blue, B = green; Mn^{2+} ions and water molecules are purple and red spheres, respectively. Metal coordination and hydrogen bond interactions are indicated by red and green dashed lines, respectively. (b) Simulated annealing omit electron density map of the HAI—FABH complex (cyan, contoured at 3.0σ), in which FABH was omitted from the structure factor calculation. Atoms are color-coded as in (a), with F = black. (c) Superposition of the HAI—ABH complex (blue), HAI—MABH complex (red), and HAI—FABH complex (green).

dx.doi.org/10.1021/jm200443b |*J. Med. Chem.* 2011, 54, 5432–5443

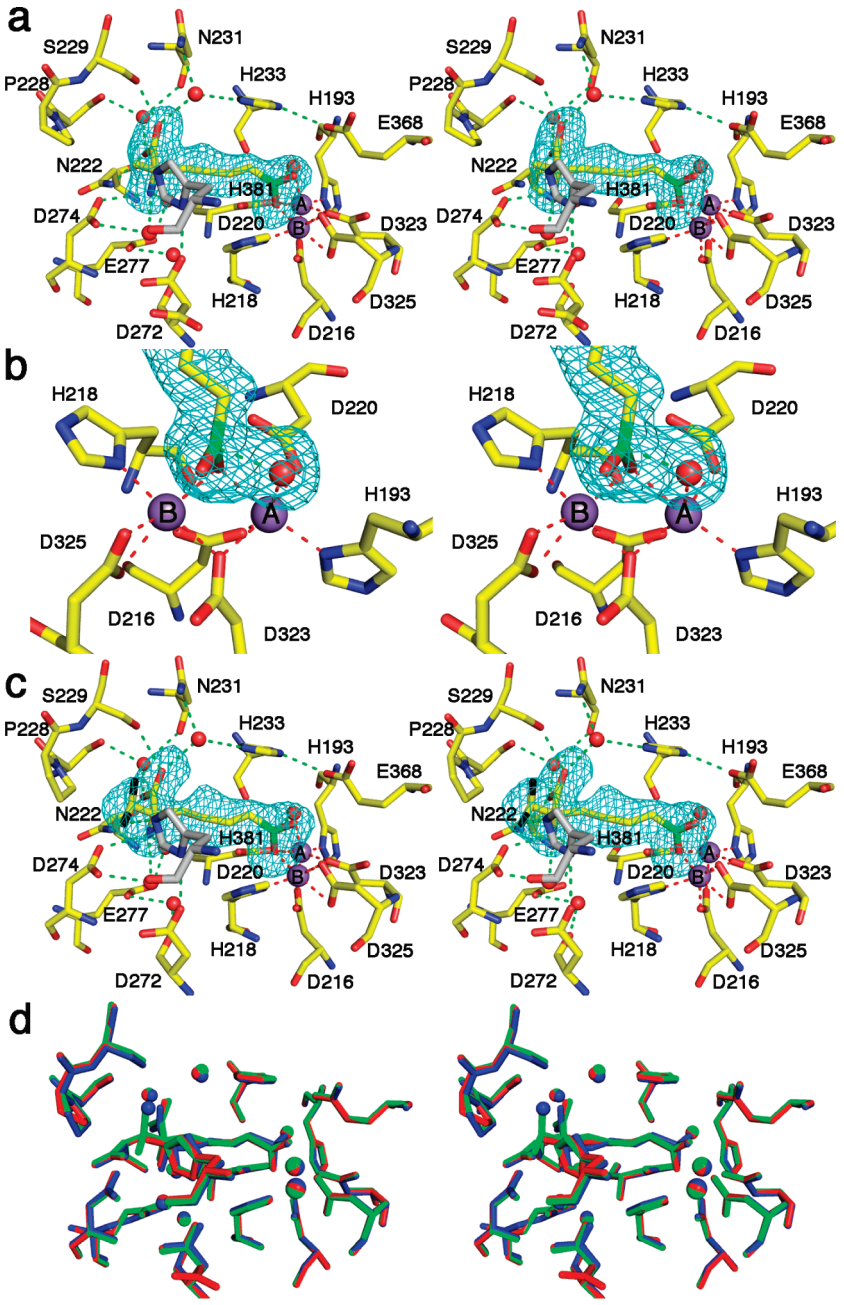

Figure 5. (a) Simulated annealing omit electron density map of the PFA−MABH complex (cyan, contoured at 3.5σ), in which MABH was omitted from the structure factor calculation. Atoms are color-coded as follows: C = yellow (C = gray for H381 from the adjacent monomer), O = red, N = blue, B = green; Mn^{2+} ions and water molecules are purple and red spheres, respectively. Red and green dashed lines indicate manganese coordination and hydrogen bond interactions, respectively. (b) Simulated annealing omit electron density map of the PFA−MABH complex (cyan, contoured at 3.5σ), in which MABH and the Mn^{2+}_A-bound water molecule were omitted from the structure factor calculation. The view is zoomed in on the binuclear manganese cluster and oriented differently from that in (a) to clearly show that the electron density is most consistent with the binding of a trigonal planar boronic acid moiety and a separate Mn^{2+}_A-bound water molecule. Similar electron density characterizes the PFA−FABH complex (data not shown). Atoms are color-coded as in (a). (c) Simulated annealing omit electron density map of the PFA−FABH complex (cyan, contoured at 3.5σ), in which FABH was omitted from the structure factor calculation. Atoms are color-coded as in (a), with F = black. (d) Superposition of the PFA−ABH complex (blue), PFA−MABH complex (red), and PFA−FABH complex (green).

DISCUSSION

In the current study, we sought to determine the structural characteristics and inhibitory properties of the most potent arginase inhibitor known to date, ABH, when the amino acid Cα-H atom is substituted with alkyl groups. On the basis of the structure of the HAI−DFMO complex, we selected the simplest alkyl substituents, CH_3 and CHF_2, to initiate this study. As discussed in detail in a recent review,[55] the replacement of hydrogen by fluorine is a commonly used strategy in medicinal chemistry to increase the lipophilicity and metabolic resistance of organic molecules. The introduction of fluorine can confer greater pharmacokinetic and pharmacodynamic stability and

dx.doi.org/10.1021/jm200443b |J. Med. Chem. 2011, 54, 5432–5443

can also influence binding affinity in that the C−F group of a fluorinated inhibitor in an enzyme−inhibitor complex can be a weak hydrogen bond acceptor.

The structures of HAI and PFA complexed with the corresponding inhibitors MABH and FABH reveal that the new α-substituent of each inhibitor is directed out toward a new region of the active site not previously identified to interact with bound inhibitors. In HAI, this region of the active site is in the vicinity of T136, so we now refer to this previously "uncharted" region of the protein surface as the "T136 region". Importantly, the current work is the first to demonstrate that the arginase active site can accommodate the binding of an α,α-disubstituted amino acid without compromising the molecular recognition of the α-amino and α-carboxylate groups, critical determinants of enzyme−inhibitor affinity.[43] Both C−F groups of FABH accept hydrogen bonds from active site solvent molecules in the HAI−FABH complex, but these interactions presumably do not contribute to enzyme−inhibitor binding affinity.

The residue corresponding to T136 of HAI in PFA is P228, so the T136 region of HAI and the corresponding "P228 region" of PFA differ in their three-dimensional contours and polarities. These regions additionally differ because of the proximity of H381 and its associated polypeptide chain in the adjacent monomer, which constricts the P228 region of PFA relative to the T136 region of HAI. If an α,α-disubstituted amino acid inhibitor can ultimately be designed to interact with the P228 region of PFA, it may be possible to develop a species-specific inhibitor of PFA that does not cross-react with HAI. Although a C−F group of FABH accepts a hydrogen bond from H381 in the PFA−FABH complex, this interaction does not enhance inhibitor binding affinity.

It is surprising that while the α-amino and α-carboxylate groups of MABH and FABH bind similarly within the active sites of HAI and PFA, both exhibit decreased inhibitory potency in comparison with ABH (Table 1). Moreover, it is particularly surprising that while each inhibitor binds with a tetrahedral boronate anion side chain to HAI, each inhibitor binds to PFA with a trigonal planar boronic acid side chain. However, neither MABH nor FABH bind to PFA as substrate analogues because of a side chain conformation that would be unattainable for substrate L-arginine. This structural feature and interactions between the newly introduced α-substituent and H381 in an adjacent subunit presumably contribute to the aberrant inhibitor binding modes and lower affinities with PFA compared with HAI. While previous studies[56] suggest that PFA may have a significant role in immune evasion and infection by the parasite *P. falciparum*, and PFA inhibition is suggested[46] as an adjuvant therapy in the treatment of malaria patients, the current work demonstrates that boronic acid analogues of ABH are not particularly effective against PFA.

The decreased affinity of MABH and FABH in comparison with the parent inhibitor ABH may be rationalized by analysis of the crystal structures of their complexes with HAI. Here, all three inhibitors clearly bind as analogues of the tetrahedral intermediate and its flanking transition state, and this feature significantly contributes to high affinity. Given the presence of potential hydrogen bonding groups in the T136 region of the HAI active site, it appears that a more polar substituent would be more favorably accommodated in this region of the active site. Additionally, a longer α-substituent might be better suited for capturing additional binding interactions in the protein landscape of T136 and beyond. Indeed, a recent report demonstrates the success of this particular strategy, with a variety of α-substituents such as $-(CH_2)_4NH_3^+$, $-(CH_2)_3OPh$, or $-(CH_2)_3$-OPh-*p*-F yielding racemic ABH derivatives with K_i values ranging from 10^{-8} to 10^{-10} M against both HAI and human arginase II.[57] Future studies will continue the exploration of structure−affinity relationships for α,α-disubstituted amino acid inhibitors bearing substituents capable of making favorable interactions in the T136 region, and such studies clearly promise to advance the development of arginase inhibitors as possible therapeutic agents.

CONCLUSIONS

This work reports the design, multistep synthesis, assay, and structural evaluation of two α,α-disubstituted amino acids, MABH and FABH, in complex with HAI and PFA. This is the first study describing the binding of α,α-disubstituted amino acids to human and parasitic arginases, and X-ray crystal structures show that the additional α-substituent is readily accommodated in each enzyme active site. These structures highlight new regions of the protein surfaces of HAI and PFA that can be targeted for additional affinity interactions. Finally, this work provides the first comparative structural insights on inhibitor discrimination between a human arginase and a parasitic arginase, which may facilitate the development of species-specific inhibitors in the search for new arginase-directed drugs.

EXPERIMENTAL SECTION

Synthesis of α,α-Disubstituted Amino Acids. General Procedures. All reagents were of at least 95% purity, purchased from Sigma Aldrich Co. and Fisher Scientific, and used as received. All solvents were of HPLC grade (Fisher Scientific or Sigma Aldrich Co). For anhydrous conditions, solvents were freshly distilled under N_2 (CH_2Cl_2 from P_2O_5, and THF from Na benzophenone). Reactions were monitored by TLC with Sigma-Aldrich aluminum plates (silica gel F_{254}, 60 Å to 0.25 mm), visualized by quenching under UV light, equilibrated in a glass chamber containing iodine, and/or stained with ninhydrin solution. Flash column chromatography was performed using Fisher Scientific silica gel 60 (230−400 mesh). High resolution mass spectrometry (HRMS) was carried out using an instrument from LCT Premier XE Micromass/Waters MS Technologies. Purities of all synthesized and tested compounds were greater than 95% based on HPLC analysis. ^{1}H and ^{13}C NMR spectra were recorded on Bruker DMX 360 and DRX 500 spectrometers at 360 and 500 MHz for ^{1}H, 90.6 and 125.6 MHz, respectively, for ^{13}C, 282 MHz for ^{19}F, and 128 MHz for ^{11}B NMR. Assignments were made based on chemical shifts, signal intensity, COSY, and HMQC sequences. ^{1}H, ^{13}C, ^{19}F, and ^{11}B NMR chemical shifts (δ) are reported in ppm relative to the residual solvent peaks. ^{1}H NMR coupling constants (J) are reported in Hz, and multiplicities are denoted as follows: s, singlet; d, doublet; t, triplet; m, multiplet; bs, broad singlet. ^{11}B NMR spectra are decoupled.

Ethyl 2-*N*-(Diphenylmethyleneamino)hex-5-enoate (2). A 10% solution of ^{t}BuOK (0.9 g, 8.25 mmol) in dry THF was added dropwise to a 10% THF solution of *N*-(diphenylmethylene)glycine ethyl ester (**1**) (2 g, 7.5 mmol) at −78 °C, with stirring under N_2. After 15 min, 4-bromobutene (2.4 mL, 22.5 mmol) in dry THF (5 mL) was added at −78 °C. After warming to room temperature, the reaction mixture was stirred for 20 h and then quenched with NH_4Cl (20 mL) and water (5 mL). The resulting immiscible layers were separated, and the aqueous layer was extracted with CH_2Cl_2 (4 × 20 mL). The combined organic extracts were washed (brine), dried (Na_2SO_4), and rotoevaporated. Purification by flash column chromatography (hexane/ethyl acetate gradients) afforded **2** as a light-yellow oil (1.8 g, 75%). ^{1}H and ^{13}C NMR ($CDCl_3$) spectra confirmed literature data.[49]

Ethyl 2-*N*-(Diphenylmethyleneamino)-2-methylhex-5-enoate (3). A solution of **2** (1.8 g, 5.6 mmol) in dry THF (20 mL) was treated successively with 10% THF solutions of ^{t}BuOK and methyl iodide, respectively (molar ratio **2**/^{t}BuOK/CH_3I 1:1.1:3). Subsequent workup and flash column chromatography (hexane/ethyl acetate gradients) yielded pure **3** as a colorless oil (1.5 g, 80%). ^{1}H NMR ($CDCl_3$): δ 7.63−7.54 (m, 2H, Ph), 7.39−7.22 (m, 6H, Ph), 7.20−7.05 (m, 2H, Ph), 5.94−5.83 (m, 1H, $-HC{=}CH_2$), 5.04 (dq, J = 1.6, 17.1, 1H, H_A, $-HC{=}CH_AH_B$), 4.98 (dd, J = 1.9, 10.2, 1H, H_B, $-HC{=}CH_AH_B$), 3.85−3.60 (m, 2H, $-O-CH_2-$), 2.40−2.25 (m, 1H, H_A, $(CH_3)C-CH_AH_B-CH_2-$), 2.22−1.94 (m, 3H, H_B, H_C, H_D, $(CH_3)C-CH_AH_B-CH_CH_D-$), 1.41 (s, 3H, $(CH_3)C-$), 1.12 (t, J = 7.1, 3H, $-CH_2-CH_3$). ^{13}C NMR ($CDCl_3$): δ 175 (CO), 166.8 (C=N), 141.5 (C_q, $C_{1\text{-Ph}}$), 139 ($-CH{=}CH_2$), 137.7 (C_q, $C_{1'\text{-Ph}}$), 130.3, 128.9, 128.8, 128.7, 128.2, 128.0 (all from Ph), 114.7 ($-CH{=}CH_2$), 66.3 (O−C), 60.6 (N−$C(CH_3)$), 42.6 ($(CH_3)C-CH_2-$), 28.8 ($(CH_3)C-$), 24.6 ($(CH_3)C-CH_2-CH_2-$), 14.1 ($-CH_2-CH_3$). HRMS m/z 336.1960 (calcd for M + H, 336.1963).

Ethyl 2-*N*-(Diphenylmethyleneamino)-2-methyl-6-(4,4,5,5-tetramethyl[1,3,2]dioxaborolan-2-yl)hex-5-enoate (5). The catalyst, a mixture of $[Ir(cod)Cl]_2$ (150 mg, 0.2 mmol) and dppm (172 mg, 0.4 mmol), was weighed in the glovebox and dissolved with stirring in dry CH_2Cl_2 (10 mL) under N_2 at room temperature. Pinacolborane (2.6 mL, 18 mmol) and then a solution of **3** (1.5 g, 4.5 mmol) in dry CH_2Cl_2 (5 mL) were added. ^{1}H NMR monitoring showed the disappearance of signals for the olefinic protons after 18 h, and the reaction mixture was then quenched with water (5 mL). After separation, the aqueous layer was extracted with Et_2O (4 × 10 mL). The combined organic layers were washed with water (5 mL), dried (Na_2SO_4), and rotoevaporated. The resulting crude orange oil was further purified by flash column chromatography (hexane/ethyl acetate gradients) and yielded **5** as a colorless oil (1.2 g, 60%). ^{1}H NMR ($CDCl_3$): δ 7.60−7.51 (m, 2H, Ph), 7.40−7.22 (m, 6H, Ph), 7.18−7.08 (m, 2H, Ph), 3.78−3.55 (m, 2H, $-O-CH_2-$), 2.05−1.80 (m, 2H, $(CH_3)C-CH_2-$), 1.52−1.45 (m, 3H, H_B, H_C, H_D, $(CH_3)C-CH_2-CH_AH_B-CH_CH_D-$), 1.42−1.35 (bs, 3H, $(CH_3)C-$), 1.25−1.15 (m, 1H, H_A, $(CH_3)C-CH_2-CH_AH_B-CH_CH_D-$), 1.23 (s, 12H, $4CH_3$ from pinacolboranyl), 1.1 (t, J = 7.1, 3H, CH_2-CH_3), 0.81 (t, J = 7.5, 2H, $-CH_2B$). ^{13}C NMR ($CDCl_3$): δ 174.4 (CO), 166.2 (C=N), 141.6 (C_q, $C_{1\text{-Ph}}$), 137.5 (C_q, $C_{1'\text{-Ph}}$), 130.2, 129.3, 129.0, 128.9, 128.3, 128.0 (all from Ph), 83.2 (2C, C_q from pinacolboranyl), 66.8 (O−C), 60.5 (N−$C(CH_3)$), 43.2 ($(CH_3)C-CH_2$), 27 ($(CH_3)C-$), 25.2 (4C, $4CH_3$ from pinacolboranyl), 24.9, 24.6 ($C(CH_3)-CH_2-CH_2-CH_2-$), 14.2 ($-CH_2-CH_3$), 11.5 (bs, CH_2-B). ^{11}B NMR ($CDCl_3$): δ 38.2. HRMS m/z 464.2979 (calcd for M + H, 464.2972).

2-Amino-6-borono-2-methylhexanoic Acid (MABH, 7). The protected derivative **5** (1.2 g, 2.6 mmol) was stirred with 6 N HCl/THF 2:1 (4 h, 70 °C), cooled to room temperature, and extracted with Et_2O (4 × 25 mL) to remove the benzophenone. The aqueous layer was rotoevaporated to dryness, retaken in 6 N HCl (50 mL), and stirred at 80−90 °C until TLC monitoring ($MeOH/CHCl_3/NH_4OH$ 8:2:0.5) revealed complete deprotection (after ∼24 h). Rotoevaporation at 40 °C, followed by flash column chromatography ($CHCl_3$/MeOH/NH_4OH gradients) afforded **7** as a white powder (0.46 g, 93%). ^{1}H NMR (D_2O): δ 1.94−1.87 (m, 1H, H_A, $(CH_3)C-CH_AH_B-$), 1.80−1.65 (m, 1H, H_B, $(CH_3)C-CH_AH_B-$), 1.47 (s, 3H, $(CH_3)C-$), 1.48−1.32 (m, 3H, H_B, H_C, H_D, $(CH_3)C-CH_2-CH_AH_B-CH_CH_D-$), 1.29−1.13 (m, 1H, $(CH_3)C-CH_2-CH_AH_B-CH_CH_D-$), 0.79 (t, J = 7.5, 2H, $-CH_2B$). ^{13}C NMR (D_2O): δ 177 (CO), 61.6 (N−$C(CH_3)$), 36.9 ($(CH_3)C-CH_2$), 25.9 ($(CH_3)C-$), 23.5, 22.5 ($(CH_3)C-CH_2-CH_2-CH_2-$), 13.9 (bs, CH_2-B). ^{11}B NMR (D_2O): δ 36.25. HRMS m/z 190.1258 (calcd for M + H, 190.1250).

Ethyl 2-*N*-(Diphenylmethyleneamino)-2-(difluoromethyl)-hex-5-enoate (4). A solution of **2** (1.8 g, 5.6 mmol) in dry THF (10 mL) was cooled to −78 °C and treated with 20% ^{t}BuOK/THF (molar ratio **2**/^{t}BuOK 1:1.1), under stirring and N_2 purging. After 20 min, chlorodifluoromethane (4.8 g, 55.5 mmol) was added to the reaction flask via needle. The resulting mixture was stirred at −78 °C (10 min), then at room temperature (45 min), quenched with brine (5 mL), and extracted with Et_2O (4 × 15 mL). The combined organic extracts were washed (brine), dried (Na_2SO_4), and rotoevaporated. The resulting yellow oil was purified (flash column chromatography, hexane/ethyl acetate gradients) to generate **4** as a colorless oil (1.4 g, 70%). ^{1}H NMR ($CDCl_3$): δ 7.69−7.05 (m, 10H), 6.17 (t, J = 55, 1H, $-CHF_2$), 5.91−5.70 (m, 1H, $-HC{=}CH_2$), 5.04 (dq, J = 1.6, 17.1, 1H, H_A, $-HC{=}CH_AH_B$), 4.95 (dd, J = 1.7, 10.2, 1H, H_B, $-HC{=}CH_AH_B$), 3.85−3.63 (m, 2H, $-O-CH_2-$), 2.45−2.20 (m, 2H, H_A, H_B, $(CHF_2)C-CH_AH_B-$), 2.18−2.09 (m, 1H, H_C, $(CHF_2)C-CH_2-CH_CH_D$), 2.06−1.95 (m, 1H, H_D, $(CHF_2)C-CH_2-CH_CH_D$), 1.12 (t, J = 7.1, 3H, $-CH_2-CH_3$). ^{13}C NMR ($CDCl_3$): δ 176.6 (CO), 169.8 (C=N), 140.3 (C_q, $C_{1\text{-Ph}}$), 138.5 ($-CH{=}CH_2$), 136.7 (C_q, $C_{1'\text{-Ph}}$), 130.9, 130.3, 129.2, 129.0, 128.5, 128.31, 128.27, 128.1 (all from Ph), 117.6 (t, $^1J_{CF}$ = 250, CHF_2), 114.9 ($-CH{=}CH_2$), 71.1 (bs, $C(CHF_2)-N$), 61.4 (O−C), 32.0 ($(CHF_2)C-CH_2$), 28.3 ($(CHF_2)C-CH_2-CH_2-$), 13.8 ($-CH_2-CH_3$). ^{19}F NMR ($CDCl_3$): δ −129.0 (ABX system 8 lines, $^2J_{FF}$ = 271, $^2J_{HF}$ = 56). HRMS m/z 372.1764 (calcd for M + H, 372.1775).

Ethyl 2-*N*-(Diphenylmethyleneamino)-2-difluoromethyl-6-(4,4,5,5-tetramethyl[1,3,2]dioxaborolan-2-yl)hex-5-enoate (6). A solution of **4** (1.4 g, 4.2 mmol) in dry CH_2Cl_2 (5 mL) was reacted with a mixture of $[Ir(cod)Cl]_2$/dppm and pinacolborane following the same experimental procedure as described for the synthesis of **5**. Flash column chromatography (pentane/Et_2O gradients) generated **6** as a colorless oil (0.95 g, 45%). ^{1}H NMR ($CDCl_3$): δ 7.65−7.11 (m, 10H), 6.16 (t, J = 56, 1H, $-CHF_2$), 3.81−3.65 (m, 2H, $-O-CH_2-$), 2.1−1.80 (m, 2H, H_A, H_B, $(CHF_2)C-CH_AH_B-$), 1.60−1.38 (m, 4H, H_C, H_D, H_E, H_F, $(CHF_2)C-CH_2-CH_CH_D-CH_EH_F-$), 1.18 (s, 6H, $2CH_3$ from pinacolboranyl), 1.16 (s, 6H, $2CH_3$ from pinacolboranyl), 1.1 (t, J = 7.1, 3H, CH_2-CH_3), 0.85−0.70 (m, 2H, $-CH_2B$). ^{13}C NMR ($CDCl_3$): δ 170.0 (CO), 169.5 (C=N), 140.3 (C_q, $C_{1\text{-Ph}}$), 136.8 (C_q, $C_{1'\text{-Ph}}$), 130.8, 129.1, 129.0, 128.4, 128.2, 128.1 (all from Ph), 83.1 (2C, C_q from pinacolboranyl), 71.1 (t, $^3J_{CF}$ = 21, $(CHF_2)C-$), 61.3 (O−C), 32.9 ($(CHF_2)C-CH_2$), 26.4 ($(CHF_2)C-CH_2-CH_2-$), 25.1 ($(CHF_2)C-CH_2-CH_2-CH_2-$), 25.0 ($2CH_3$ from pinacolboranyl), 24.9 ($2CH_3$ from pinacolboranyl), 13.9 ($-CH_2-CH_3$), 11.3 (CH_2-B). ^{11}B NMR ($CDCl_3$): δ 32.5. ^{19}F NMR ($CDCl_3$): δ −129.3 (ABX system, eight lines, $^2J_{FF}$ = 274, $^2J_{HF}$ = 56.5). HRMS m/z 500.2772 (calcd for M + H, 500.2783).

2-Amino-6-borono-2-(difluoromethyl)hexanoic Acid (FABH, 8). Intermediate **6** (0.9 g, 1.8 mmol) was deprotected by the same experimental protocol utilized for the deprotection of **5**. Flash column chromatography ($CHCl_3$/MeOH/NH_4OH/^{i}PrOH gradients) afforded **8** as a white precipitate (0.37 g, 92%). ^{1}H NMR (D_2O): δ 6.19 (t, J = 54, 1H, $-CHF_2$), 1.96−1.88 (m, 1H, H_A, $(CHF_2)C-CH_AH_B$), 1.78−1.68 (m, 1H, H_B, $(CHF_2)C-CH_AH_B$), 1.53−1.30 (m, 3H, H_B, H_C, H_D, $(CHF_2)C-CH_2-CH_AH_B-CH_CH_D-$), 1.30−1.08 (m, 1H, $(CHF_2)C-CH_2-CH_AH_B-CH_CH_D-$), 0.76 (t, J = 7.5, 2H, $-CH_2B$). ^{13}C NMR (D_2O): δ 171.5 (d, $^4J_{CF}$ = 6.1, CO), 116.0 (t, $^1J_{CF}$ = 246, CHF_2), 65.5 (dd, $^3J_{CF}$ = 16.5, 20, $(CHF_2)C-$), 31.2 (d, $^4J_{CF}$ = 3.2, $(CHF_2)C-CH_2$), 25.1 ($(CHF_2)C-CH_2-CH_2-$), 23.4 ($(CHF_2)C-CH_2-CH_2-CH_2-$), 13.7 (bs, CH_2-B). ^{11}B NMR (D_2O): δ 21.6. ^{19}F NMR (D_2O): δ −130.0 (ABX system, eight lines, $^2J_{FF}$ = 278, $^2J_{HF}$ = 54). HRMS m/z 226.1057 (calcd for M + H, 226.1062).

Surface Plasmon Resonance (SPR). The binding affinities of MABH and FABH to HAI were determined by SPR on a Biacore 3000 instrument according to a previously reported procedure[58] except that all measurements were made at pH 8.5 and inhibitor concentrations were 0−200 nm for ABH, 0−25 μM for MABH, and 0−500 μM for FABH. In this measurement, HAI is immobilized on carboxymethylated

Table 2. X-ray Crystallographic Data Collection and Refinement Statistics

parameter	complex					
	HAI−DFMO	HAI−L-Orn	HAI−MABH	HAI−FABH	PFA−MABH	PFA−FABH
resolution limit, Å	50−1.70	50−1.43	50−1.60	50−1.70	50−1.90	50−2.0
total/unique reflections	129926/67814	233126/116771	82598/8046	128641/68384	404894/44684	412761/38494
completeness (%) (overall/outer shell)	99.9/100.0	99.8/100.0	98.4/95.6	99.0/98.2	99.9/99.2	99.9/98.7
R_{merge} (overall/outer shell)[a]	0.101/0.412	0.067/0.640	0.050/0.298	0.148/0.577	0.081/0.444	0.090/0.587
$I/\sigma(I)$ (overall/outer shell)	11.0/2.7	35.6/2.0	25.1/2.7	11.6/2.3	23.0/3.4	23.6/2.7
	Refinement					
R/R_{free}	0.161/0.202[b]	0.147/0.185[b]	0.129/0.163[b]	0.136/0.178[b]	0.163/0.182[c]	0.167/0.183[c]
protein atoms[d]	4782	4782	4764	4778	2416	2416
manganese ions[d]	4	4	4	4	2	2
ligand atoms[d]	24	18	28	32	13	15
water molecules[d]	345	393	765	760	212	203
rms deviation						
bond length, Å	0.005	0.006	0.006	0.006	0.007	0.006
bond angle, deg	1.3	1.4	1.0	1.0	1.1	0.9
dihedral angle, deg	23	23	17	18	13	13
PDB accession code	3GN0	3GMZ	3SJT	3SKK	3SL1	3SL0

[a] $R_{merge} = \Sigma|I - \langle I\rangle|/\Sigma I$, where I is the observed intensity and $\langle I\rangle$ is the average intensity calculated for replicate data. [b] $R_{twin} = \Sigma|[|F_{calc/A}|^2 + |F_{calc/B}|^2]^{1/2} - |F_{obs}||/\Sigma|F_{obs}|$ for reflections contained in the working set. $|F_{obs}|$ is the observed structural factor amplitude, and $|F_{calc/A}|$ and $|F_{calc/B}|$are the structure factor amplitudes calculated for twin domains A and B, respectively. R_{twin} underestimates the residual error in the model over the two twin-related reflections by a factor of approximately 0.7. The same expression describes $R_{twin/free}$, calculated for test set reflections excluded from refinement. [c] $R = \Sigma||F_{obs}| - |F_{calc}||/\Sigma|F_{obs}|$, where $|F_{obs}|$ and $|F_{calc}|$ are the observed and calculated structure factor amplitudes, respectively. The same expression describes R_{free}, calculated for test set reflections excluded from refinement. [d] Per asymmetric unit.

dextran over the gold surface of sensor chip CM5 and the inhibitor is added to a buffer solution that continuously flows over the sensor surface. Inhibitor binding to the immobilized enzyme causes a change in the angle of reflection of polarized light used to interrogate the glass sensor support. Angular changes are recorded in real time as "response units" in the sensorgrams shown in Figure 3; these changes are proportional to the concentration of enzyme-bound inhibitor and thus allow for real time monitoring of the enzyme−inhibitor interaction as a function of inhibitor concentration. Dissociation constants are calculated using a 1:1 Langmuir interaction model.[59]

Enzyme Inhibition Assay. The inhibition of PFA by MABH and FABH was analyzed using a colorimetric method,[60] as previously described.[40] Briefly, the reaction of urea with α-isonitrosopropiophenone was measured at a wavelength of 550 nm using the Envision plate reader (courtesy of Dr. Scott Diamond, Institute of Medicine and Engineering, University of Pennsylvania). The arginase reaction was performed in 50 mM Tris (pH 8.0), 0.5 mM TCEP, 1 mM $MnCl_2$, 0.2 μM protein, 0−100 mM inhibitor, and 20 mM L-arginine for 5−16 min at 37 °C. Assay mixture and protein were preincubated at 37 °C for 1 min before initiating the reaction. The assay mixture (20 μL) was stopped with a sulfuric−phosphoric acid/α-isonitrosopropiophenone mixture (140 μL). Reaction points were developed in a thermocycler (90 °C, 1 h), followed by incubation at 21 °C (15 min). The K_i values for the racemic mixtures of MABH and FABH were calculated using the Cheng−Prusoff equation[61] with the software Graphpad Prism (2008).

Crystallography: HAI Complexes. Crystals of the HAI−DFMO and HAI−L-ornithine complexes were prepared by soaking crystals of unliganded HAI prepared as described[42] in 0.1 M bis-Tris (pH 6.5), 20% PEG monomethyl ether, and 20 mM DFMO or 20 mM L-ornithine for 2 days. Crystals of the HAI−MABH and HAI−FABH complexes were prepared by cocrystallization in hanging drops at 21 °C. Drops containing 3 μL of protein solution [3.5 mg/mL HAI, 50 mM bicine (pH 8.5), 2 mM MABH, 100 μM $MnCl_2$] and 3 μL of precipitant solution [0.1 M HEPES (pH 7.0), 22−28% Jeffamine] were equilibrated against a 1 mL reservoir of precipitant solution. Crystals appeared overnight and grew with typical dimensions of 0.5 mm × 0.2 mm × 0.2 mm. All crystals were cryoprotected in a precipitant solution containing 32% Jeffamine prior to flash cooling in liquid nitrogen.

X-ray diffraction data from all crystals were collected at GM/CA-CAT beamline 23-ID-D or NE-CAT beamline 24-ID-C at the Advanced Photon Source (APS, Argonne, IL). Diffraction intensities measured from crystals of HAI complexes exhibited symmetry consistent with apparent space group $P6$ (unit cell parameters $a = b = 90.3$ Å, $c = 69.3$ Å). Intensity data integration and reduction were performed using the HKL2000 suite of programs.[62] Data reduction statistics are recorded in Table 2. As with crystals of other HAI complexes,[38,42] deviations from ideal Wilson statistics were observed with $\langle I^2\rangle/\langle I\rangle^2 = 1.5$, indicating perfect hemihedral twinning.[63] The structure of each enzyme−ligand complex was solved by molecular replacement using the program Phaser[64] with chain A of unliganded HAI (PDB accession code 2ZAV, less water molecules)[42] used as a search probe against twinned data. In order to calculate electron density maps, structure factor amplitudes ($|F_{obs}|$) derived from twinned data ($|I_{obs}|$) were deconvoluted into structure factor amplitudes corresponding to twin domains A and B ($|F_{obs/A}|$ and $|F_{obs/B}|$, respectively) using the structure-based algorithm of Redinbo and Yeates[63] implemented in CNS.[65] Electron density maps were visualized with the graphics software COOT.[66] After initial rigid body refinement with CNS,[65] refinement of each complex was performed against twinned data using PHENIX.[67] After water molecules were located and fit into the map, gradient omit maps revealed the bound ligand in the active site of each monomer in the asymmetric unit. Ligand atoms were refined with full occupancy and exhibited atomic B factors consistent with the average B-factor calculated for the entire protein. The quality of each final model was assessed using PROCHECK.[68] Final refinement statistics are recorded in Table 2.

Crystallography: *Plasmodium falciparum* Arginase Complexes. Recombinant PFA was prepared and purified as described, and crystals of complexes with MABH and FABH were prepared using conditions similar to those employed in the structure determination of the PFA−ABH complex.[40] Briefly, a 2 μL sitting drop of enzyme−inhibitor complex [5 mg/mL PFA, 50 mM Tris (pH 8.0), 200 mM NaCl, 1 mM $MnCl_2$, 1 mM tris(2-carboxyethyl)phosphine (TCEP), 5 mM inhibitor] was mixed with a 2 μL drop of precipitant solution [1.2 M sodium/potassium phosphate (pH 8.0)] and equilibrated against 500 μL of precipitant solution in the reservoir at 21 °C. Crystals appeared within 1−2 days and were harvested, cryoprotected in 30% Jeffamine ED-2001, 0.1 M HEPES (pH 7.0), 50 μM inhibitor, and flash-cooled in liquid nitrogen. Diffraction data were measured on NE-CAT beamline 24-ID-E at APS. Data collection statistics are recorded in Table 2.

Data were indexed and merged using HKL2000.[62] Molecular replacement calculations were performed with PHASER[64] using the atomic coordinates of PFA less inhibitor and solvent atoms (PDB accession code 3MMR)[40] as a search probe for rotation and translation function calculations. Iterative cycles of refinement and model building were performed using PHENIX[67] and COOT,[66] respectively, in order to improve each structure as guided by R_{free}. Refinement included six defined TLS groups identified by the TLS motion determination server.[69] As also observed in the PFA−ABH complex,[40] the N-terminus was disordered (continuous main chain electron density starts at K22) and residues G72−N153 in the L2 loop were disordered. The quality of each final model was assessed using PROCHECK.[68] Refinement statistics are recorded in Table 2.

Accession Codes

†Atomic coordinates of human arginase I complexes with DFMO, L-ornithine, MABH, and FABH have been deposited in the Protein Data Bank (www.rcsb.org) with accession codes 3GN0, 3GMZ, 3SJT, and 3SKK, respectively; coordinates of *P. falciparum* arginase complexes with MABH and FABH have been deposited with accession codes 3SL1 and 3SL0, respectively.

AUTHOR INFORMATION

Corresponding Author

*Phone: 215-898-5714. Fax: 215-573-2201. E-mail: chris@sas.upenn.edu.

ACKNOWLEDGMENT

These studies were supported by NIH Grant GM49758. We thank Dr. Richard Pottorf of Provid Pharmaceuticals, Inc., for helpful discussions; Dr. Steven Seeholzer, Dr. Hua Ding, and the Protein Core Facility at Children's Hospital of Philadelphia, PA, for assistance with surface plasmon resonance measurements; Dr. Scott Diamond at the Institute of Medicine and Engineering, University of Pennsylvania, for assistance with kinetic colorimetric assays; and Dr. Rakesh Kohli for recording the high resolution mass spectra. We also thank the Northeastern Collaborative Access Team (NE-CAT) and the National Institute of General Medical Sciences and National Cancer Institute Collaborative Access Team (GM/CA-CAT) for beamlines at the APS and for access to X-ray crystallographic data collection facilities. Use of the Advanced Photon Source is supported by Award RR-15301 from the National Center for Research Resources at the National Institutes of Health and by the U.S. Department of Energy, Office of Basic Energy Sciences, under Contract No. DE-AC02-06CH11357.

ABBREVIATIONS USED

ABH, 2-(*S*)-amino-6-boronohexanoic acid; APS, Advanced Photon Source; BEC, *S*-(2-boronoethyl)-L-cysteine; DFMO, 2-(difluoromethyl)-L-ornithine; FABH, 2-amino-6-borono-2-(difluoromethyl)-hexanoic acid; HAI, human arginase I; HRMS, high resolution mass spectrometry; MABH, 2-amino-6-borono-2-methylhexanoic acid; NO, nitric oxide; PFA, *Plasmodium falciparum* arginase; SPR, surface plasmon resonance

REFERENCES

(1) Grody, W. W.; Dizikes, G. J.; Cederbaum, S. D. Human arginase isozymes. *Isozymes: Curr. Top. Biol. Med. Res.* **1987**, *13*, 181–214.

(2) Jenkinson, C. P.; Grody, W. W.; Cederbaum, S. D. Comparative properties of arginases. *Comp. Biochem. Physiol., Part B: Biochem. Mol. Biol.* **1996**, *114*, 107–132.

(3) Wu, G.; Morris, S. M. Arginine metabolism: nitric oxide and beyond. *Biochem. J.* **1998**, *336* (Part 1), 1–17.

(4) Morris, S. M., Jr. Regulation of enzymes of the urea cycle and arginine metabolism. *Annu. Rev. Nutr.* **2002**, *22*, 87–105.

(5) Morris, S. M., Jr. Recent advances in arginine metabolism: roles and regulation of the arginases. *Br. J. Pharmacol.* **2009**, *157*, 922–930.

(6) Borcic, O.; Straus, B. Separation of arginase isoenzymes from human tissues by agar gel electrophoresis. *J. Clin. Chem. Clin. Biochem.* **1976**, *14*, 533–535.

(7) Herzfeld, A.; Raper, S. M. The heterogeneity of arginases in rat tissues. *Biochem. J.* **1976**, *153*, 469–478.

(8) Morris, S. M., Jr.; Bhamidipati, D.; Kepka-Lenhart, D. Human type II arginase: sequence analysis and tissue-specific expression. *Gene* **1997**, *193*, 157–161.

(9) Gotoh, T.; Araki, M.; Mori, M. Chromosomal localization of the human arginase II gene and tissue distribution of its mRNA. *Biochem. Biophys. Res. Commun.* **1997**, *233*, 487–491.

(10) Modolell, M.; Corraliza, I. M.; Link, F.; Soler, G.; Eichmann, K. Reciprocal regulation of the nitric oxide synthase/arginase balance in mouse bone marrow-derived macrophages by TH1 and TH2 cytokines. *Eur. J. Immunol.* **1995**, *25*, 1101–1104.

(11) Hesse, M.; Modolell, M.; La Flamme, A. C.; Schito, M.; Fuentes, J. M.; Cheever, A. W.; Pearce, E. J.; Wynn, T. A. Differential regulation of nitric oxide synthase-2 and arginase-1 by type 1/type 2 cytokines in vivo: granulomatous pathology is shaped by the pattern of L-arginine metabolism. *J. Immunol.* **2001**, *167*, 6533–6544.

(12) Wang, W. W.; Jenkinson, C. P.; Griscavage, J. M.; Kern, R. M.; Arabolos, N. S.; Byrns, R. E.; Cederbaum, S. D.; Ignarro, L. J. Co-induction of arginase and nitric oxide synthase in murine macrophages activated by lipopolysaccharide. *Biochem. Biophys. Res. Commun.* **1995**, *210*, 1009–1016.

(13) Chakder, S.; Rattan, S. L-Arginine deficiency causes suppression of nonadrenergic noncholinergic nerve-mediated smooth muscle relaxation: role of L-citrulline recycling. *J. Pharmacol. Exp. Ther.* **1997**, *282*, 378–384.

(14) Baggio, R.; Emig, F. A.; Christianson, D. W.; Ash, D. E.; Chakder, S.; Rattan, S. Biochemical and functional profile of a newly developed potent and isozyme-selective arginase inhibitor. *J. Pharmacol. Exp. Ther.* **1999**, *290*, 1409–1416.

(15) Cox, J. D.; Kim, N. N.; Traish, A. M.; Christianson, D. W. Arginase−boronic acid complex highlights a physiological role in erectile function. *Nat. Struct. Biol.* **1999**, *6*, 1043–1047.

(16) Smith, R. J.; Phang, J. M. The importance of ornithine as a precursor for proline in mammalian cells. *J. Cell. Physiol.* **1979**, *98*, 475–481.

(17) Albina, J. E.; Abate, J. A.; Mastrofrancesco, B. Role of ornithine as a proline precursor in healing wounds. *J. Surg. Res.* **1993**, *55*, 97–102.

(18) Singh, R.; Pervin, S.; Karimi, A.; Cederbaum, S.; Chaudhuri, G. Arginase activity in human breast cancer cell lines: N^{ω}-hydroxy-L-arginine selectively inhibits cell proliferation and induces apoptosis in MDA-MB-468 cells. *Cancer Res.* **2000**, *60*, 3305–3312.

(19) Wei, L. H.; Wu, G.; Morris, S. M., Jr.; Ignarro, L. J. Elevated arginase I expression in rat aortic smooth muscle cells increases cell proliferation. *Proc. Natl. Acad. Sci. U.S.A.* **2001**, *98*, 9260–9264.

(20) Auvinen, M.; Paasinen, A.; Andersson, L. C.; Hölttä, E. Ornithine decarboxylase activity is critical for cell transformation. *Nature* **1992**, *360*, 355–358.

(21) Bivalacqua, T. J.; Hellstrom, W. J.; Kadowitz, P. J.; Champion, H. C. Increased expression of arginase II in human diabetic corpus cavernosum: in diabetic-associated erectile dysfunction. *Biochem. Biophys. Res. Commun.* **2001**, *283*, 923–927.

(22) Bivalacqua, T. J.; Burnett, A. L.; Hellstrom, W. J.; Champion, H. C. Overexpression of arginase in the aged mouse penis impairs erectile function and decreases eNOS activity: influence of in vivo gene therapy of anti-arginase. *Am. J. Physiol.: Heart Circ. Physiol.* **2007**, *292*, H1340–H1351.

(23) Zimmermann, N.; King, N. E.; Laporte, J.; Yang, M.; Mishra, A.; Pope, S. M.; Muntel, E. E.; Witte, D. P.; Pegg, A. A.; Foster, P. S.; Hamid, Q.; Rothenberg, M. E. Dissection of experimental asthma with DNA microarray analysis identifies arginase in asthma pathogenesis. *J. Clin. Invest.* **2003**, *111*, 1863–1874.

(24) Pauleau, A. L.; Rutschman, R.; Lang, R.; Pernis, A.; Watowich, S. S.; Murray, P. J. Enhancer-mediated control of macrophage-specific arginase I expression. *J. Immunol.* **2004**, *172*, 7565–7573.

(25) Zimmermann, N.; Mishra, A.; King, N. E.; Fulkerson, P. C.; Doepker, M. P.; Nikolaidis, N. M.; Kindinger, L. E.; Moulton, E. A.; Aronow, B. J.; Rothenberg, M. E. Transcript signatures in experimental asthma: identification of STAT6-dependent and -independent pathways. *J. Immunol.* **2004**, *172*, 1815–1824.

(26) Bergeron, C.; Boulet, L. P.; Page, N.; Laviolette, M.; Zimmermann, N.; Rothenberg, M. E.; Hamid, Q. Influence of cigarette smoke on the arginine pathway in asthmatic airways: increased expression of arginase I. *J. Allergy Clin. Immunol.* **2007**, *119*, 391–397.

(27) North, M. L.; Khanna, N.; Marsden, P. A.; Grasemann, H.; Scott, J. A. Functionally important role for arginase 1 in the airway hyperresponsiveness of asthma. *Am. J. Physiol.: Lung Cell. Mol. Physiol.* **2009**, *296*, L911–920.

(28) Li, H.; Romieu, I.; Sienra-Monge, J. J.; Ramirez-Aguilar, M.; Estela Del Rio-Navarro, B.; Kistner, E. O.; Gjessing, H. K.; Lara-Sanchez Idel, C.; Chiu, G. Y.; London, S. J. Genetic polymorphisms in arginase I and II and childhood asthma and atopy. *J. Allergy Clin. Immunol.* **2006**, *117*, 119–126.

(29) Litonjua, A. A.; Lasky-Su, J.; Schneiter, K.; Tantisira, K. G.; Lazarus, R.; Klanderman, B.; Lima, J. J.; Irvin, C. G.; Peters, S. P.; Hanrahan, J. P.; Liggett, S. B.; Hawkins, G. A.; Meyers, D. A.; Bleecker, E. R.; Lange, C.; Weiss, S. T. ARG1 is a novel bronchodilator response gene: screening and replication in four asthma cohorts. *Am. J. Respir. Crit. Care Med.* **2008**, *178*, 688–694.

(30) Maarsingh, H.; Zaagsma, J.; Meurs, H. Arginine homeostasis in allergic asthma. *Eur. J. Pharmacol.* **2008**, *585*, 375–384.

(31) Maarsingh, H.; Zaagsma, J.; Meurs, H. Arginase: a key enzyme in the pathophysiology of allergic asthma opening novel therapeutic perspectives. *Br. J. Pharmacol.* **2009**, *158*, 652–664.

(32) North, M. L.; Meurs, H.; Zaagsma, J.; Scott, J. A.; Maarsingh, H. Arginase in asthma: recent developments in animal and human studies. *Open Nitric Oxide J.* **2010**, *2*, 20–36.

(33) Cama, E.; Colleluori, D. M.; Emig, F. A.; Shin, H.; Kim, S. W.; Kim, N. N.; Traish, A. M.; Ash, D. E.; Christianson, D. W. Human arginase II: crystal structure and physiological role in male and female sexual arousal. *Biochemistry* **2003**, *42*, 8445–8451.

(34) Maarsingh, H.; Zuidhof, A. B.; Bos, I. S.; van Duin, M.; Boucher, J. L.; Zaagsma, J.; Meurs, H. Arginase inhibition protects against allergen-induced airway obstruction, hyperresponsiveness, and inflammation. *Am. J. Respir. Crit. Care Med.* **2008**, *178*, 565–573.

(35) Ilies, M.; Di Costanzo, L.; North, M. L.; Scott, J. A.; Christianson, D. W. 2-Aminoimidazole amino acids as inhibitors of the binuclear manganese metalloenzyme human arginase I. *J. Med. Chem.* **2010**, *53*, 4266–4276.

(36) Ryoo, S.; Gupta, G.; Benjo, A.; Lim, H. K.; Camara, A.; Sikka, G.; Sohi, J.; Santhanam, L.; Soucy, K.; Tuday, E.; Baraban, E.; Ilies, M.; Gerstenblith, G.; Nyhan, D.; Shoukas, A.; Christianson, D. W.; Alp, N. J.; Champion, H. C.; Huso, D.; Berkowitz, D. E. Endothelial arginase II: a novel target for the treatment of atherosclerosis. *Circ. Res.* **2008**, *102*, 923–932.

(37) Baggio, R.; Elbaum, D.; Kanyo, Z. F.; Carroll, P. J.; Cavalli, R. C.; Ash, D. E.; Christianson, D. W. Inhibition of Mn^{2+}_2-arginase by borate leads to the design of a transition state analogue inhibitor, 2(*S*)-amino-6-boronohexanoic acid. *J. Am. Chem. Soc.* **1997**, *119*, 8107–8108.

(38) Di Costanzo, L.; Sabio, G.; Mora, A.; Rodriguez, P. C.; Ochoa, A. C.; Centeno, F.; Christianson, D. W. Crystal structure of human arginase I at 1.29-Å resolution and exploration of inhibition in the immune response. *Proc. Natl. Acad. Sci. U.S.A.* **2005**, *102*, 13058–13063.

(39) Colleluori, D. M.; Ash, D. E. Classical and slow-binding inhibitors of human type II arginase. *Biochemistry* **2001**, *40*, 9356–9362.

(40) Dowling, D. P.; Ilies, M.; Olszewski, K. L.; Portugal, S.; Mota, M. M.; Llinás, M.; Christianson, D. W. Crystal structure of arginase from *Plasmodium falciparum* and implications for L-arginine depletion in malarial infection. *Biochemistry* **2010**, *49*, 5600–5608.

(41) Kanyo, Z. F.; Scolnick, L. R.; Ash, D. E.; Christianson, D. W. Structure of a unique binuclear manganese cluster in arginase. *Nature* **1996**, *383*, 554–557.

(42) Di Costanzo, L.; Pique, M. E.; Christianson, D. W. Crystal structure of human arginase I complexed with thiosemicarbazide reveals an unusual thiocarbonyl μ-sulfide ligand in the binuclear manganese cluster. *J. Am. Chem. Soc.* **2007**, *129*, 6388–6389.

(43) Shishova, E. Y.; Di Costanzo, L.; Emig, F. A.; Ash, D. E.; Christianson, D. W. Probing the specificity determinants of amino acid recognition by arginase. *Biochemistry* **2009**, *48*, 121–131.

(44) Busnel, O.; Carreaux, F.; Carboni, B.; Pethe, S.; Goff, S. V.; Mansuy, D.; Boucher, J.-L. Synthesis and evaluation of new ω-boronoα-amino acids as rat liver arginase inhibitors. *Bioorg. Med. Chem.* **2005**, *13*, 2373–2379.

(45) Collet, S.; Carreaux, F.; Boucher, J.-L.; Pethe, S.; Lepoivre, M.; Danion-Bougot, R.; Danion, D. Synthesis and evaluation of ω-boronoα-amino acids as active-site probes of arginase and nitric oxide synthases. *J. Chem. Soc., Perkin Trans. 1* **2000**, 177–182.

(46) Yeo, T. W.; Lampah, D. A.; Gitawati, R.; Tjitra, E.; Kenangalem, E.; McNeil, Y. R.; Darcy, C. J.; Granger, D. L.; Weinberg, J. B.; Lopansri, B. K.; Price, R. N.; Duffull, S. B.; Celermajer, D. S.; Anstey, N. M. Recovery of endothelial function in severe falciparum malaria: relationship with improvement in plasma L-arginine and blood lactate concentrations. *J. Infect. Dis.* **2008**, *198*, 602–608.

(47) Selamnia, M.; Mayeur, C.; Robert, V.; Blachier, F. α-Difluoromethylornithine (DFMO) as a potent arginase activity inhibitor in human colon carcinoma cells. *Biochem. Pharmacol.* **1998**, *55*, 1241–1251.

(48) Reczkowski, R. S.; Ash, D. E. Rat liver arginase: kinetic mechanism, alternate substrates, and inhibitors. *Arch. Biochem. Biophys.* **1994**, *312*, 31–37.

(49) Andrei, D.; Wnuk, S. F. *S*-Adenosylhomocysteine analogues with the carbon-5′ and sulfur atoms replaced by a vinyl unit. *Org. Lett.* **2006**, *8*, 5093–5096.

(50) Stork, G.; Leong, A. Y.; Touzin, A. M. Alkylation and Michael additions of glycine ethyl ester. Use in α-amino acid synthesis and as acyl carbanion equivalent. *J. Org. Chem.* **1976**, *41*, 3491–3493.

(51) Rubio, A.; Ezquerra, J. First Michael addition reaction of α-substituted *N*-diphenylmethyleneglycinate with ethyl propiolate. Synthesis of α-substituted (*E*)-3,4-dehydroglutamic acids. *Tetrahedron Lett.* **1995**, *36*, 5823–5826.

(52) O'Donnell, M. J. The enantioselective synthesis of α-amino acids by phase-transfer catalysis with achiral Schiff base esters. *Acc. Chem. Res.* **2004**, *37*, 506–517.

(53) Bey, P.; Vevert, J. P.; Van Dorsselaer, V.; Kolb, M. Direct synthesis of α-halogenomethyl-α-amino acids from the parent α-amino acids. *J. Org. Chem.* **1979**, *44*, 2732–2742.

(54) Yamamoto, Y.; Fujikawa, R.; Umemoto, T.; Miyaura, N. Iridium-catalyzed hydroboration of alkenes with pinacolborane. *Tetrahedron* **2004**, *60*, 10695–10700.

(55) Ma, J.-A.; Cahard, D. Update 1 of: asymmetric fluorination, trifluoromethylation, and perfluoroalkylation reactions. *Chem. Rev.* **2008**, *108*, PR1–43.

(56) Olszewski, K. L.; Morrisey, J. M.; Wilinski, D.; Burns, J. M.; Vaidya, A. B.; Rabinowitz, J. D.; Llinás, M. Host−parasite interactions

revealed by *Plasmodium falciparum* metabolomics. *Cell Host Microbe* **2009**, *5*, 191–199.

(57) Christianson, D. W.; Tomczuk, B. E.; Pottorf, R. S.; Colasanti, A. V.; Olson, G. L. Arginase Inhibitors and Methods of Use International Patent Application. WO 2010/085797 A2, 2010; University of Pennsylvania and Arginetix, Inc., 162 pp.

(58) Cama, E.; Shin, H.; Christianson, D. W. Design of amino acid sulfonamides as transition-state analogue inhibitors of arginase. *J. Am. Chem. Soc.* **2003**, *125*, 13052–13057.

(59) Schuck, P. Use of surface plasmon resonance to probe the equilibrium and dynamic aspects of interactions between biological macromolecules. *Annu. Rev. Biophys. Biomol. Struct.* **1997**, *26*, 541–566.

(60) Archibald, R. M.; Ortiz, P.; Stroh, E.; Bronner, J. Colorimetric determination of urea. *J. Biol. Chem.* **1945**, *157*, 507–518.

(61) Cheng, Y.-C.; Prusoff, W. H. Relation between the inhibition constant (K_I) and the concentration of inhibitor which causes 50 per cent inhibition (I_{50}) of an enzymic reaction. *Biochem. Pharmacol.* **1973**, *22*, 3099–3108.

(62) Otwinowski, Z.; Minor, W. Processing of X-ray diffraction data collected in oscillation mode. *Methods Enzymol.* **1997**, *276*, 307–326.

(63) Yeates, T. O. Detecting and overcoming crystal twinning. *Methods Enzymol.* **1997**, *276*, 344–358.

(64) McCoy, A. J.; Grosse-Kunstleve, R. W.; Adams, P. D.; Winn, M. D.; Storoni, L. C.; Read, R. J. Phaser crystallographic software. *J. Appl. Crystallogr.* **2007**, *40*, 658–674.

(65) Brünger, A. T.; Adams, P. D.; Clore, G. M.; DeLano, W. L.; Gros, P.; Grosse-Kunstleve, R. W.; Jiang, J.-S.; Kuszewski, J.; Nilges, M.; Pannu, N. S.; Read, R. J.; Rice, L. M.; Simonson, T.; Warren, G. L. Crystallography & NMR system: a new software suite for macromolecular structure determination. *Acta Crystallogr., Sect. D: Biol. Crystallogr.* **1998**, *54*, 905–921.

(66) Emsley, P.; Cowtan, K. Coot: model-building tools for molecular graphics. *Acta Crystallogr., Sect. D: Biol. Crystallogr.* **2004**, *60*, 2126–2132.

(67) Adams, P. D.; Afonine, P. V.; Bunkóczi, G.; Chen, V. B.; Davis, I. W.; Echols, N.; Headd, J. J.; Hung, L. W.; Kapral, G. J.; Grosse-Kunstleve, R. W.; McCoy, A. J.; Moriarty, N. W.; Oeffner, R.; Read, R. J.; Richardson, D. C.; Richardson, J. S.; Terwilliger, T. C.; Zwart, P. H. PHENIX: a comprehensive Python-based system for macromolecular structure solution. *Acta Crystallogr., Sect. D: Biol. Crystallogr.* **2010**, *D66*, 213–221.

(68) Laskowski, R. A.; MacArthur, M. W.; Moss, D. S.; Thornton, J. M. PROCHECK: a program to check the stereochemical quality of protein structures. *J. Appl. Crystallogr.* **1993**, *26*, 283–291.

(69) Painter, J.; Merritt, E. A. TLSMD Web server for the generation of multi-group TLS models. *J. Appl. Crystallogr.* **2006**, *39*, 109–111.